Direct numerical simulation, large eddy simulation and unsteady Reynolds-averaged Navier–Stokes simulations of periodic unsteady flow in a low-pressure turbine cascade: A comparison

V Michelassi, J. G. Wissink and W Rodi

Proceedings of the Institution of Mechanical Engineers, Part A: Journal of Power and Energy 2003 217: 403
DOI: 10.1243/095765003322315469

Direct numerical simulation, large eddy simulation and unsteady Reynolds-averaged Navier–Stokes simulations of periodic unsteady flow in a low-pressure turbine cascade: a comparison

V Michelassi[1], **J G Wissink**[2] and **W Rodi**[2]*
[1]Dipartimento di Ingegneria Meccanica e Industriale, Università Roma Tre, Italy
[2]Institut für Hydromechanik, Universität Karlsruhe, Germany

Abstract: The unsteady periodic flow in a low-pressure (LP) prismatic turbine vane with incoming wakes is computed by direct numerical simulation (DNS), large eddy simulation (LES) and unsteady Reynolds-averaged Navier–Stokes simulations (URANSs). The results are compared with existing measurements at a Reynolds number $Re = 5.18 \times 10^4$ which reveal the presence of a large unsteady stalled region on the suction side. Both DNS and LES suggest that the boundary layer separates while being still laminar, with subsequent turbulent reattachment. Several URANSs with and without a transition model and a constraint on the turbulence time-scale designed to prevent excessive production in the stagnation region are analysed and compared with the DNS and LES. The useful information provided by DNS and LES has made it possible to improve the results of the URANSs, which ensure a fair reproduction of the flow, especially in terms of blade load and losses, although they partly fail to detail the complex wake–boundary layer interaction in the separated flow region.

Keywords: numerical simulation, low-pressure turbine, transition, turbulence

1 INTRODUCTION

The accurate prediction of the unsteady flow around turbine and/or compressor blades with incoming wakes largely depends on the ability of the computational model to predict transition from laminar to turbulent flow. Mayle [**1**], while reviewing the transition data and models pertaining to the turbomachinery field, distinguished between three types of transition mechanism: natural, bypass and separated flow. Natural transition is unlikely to occur in a turbomachine owing to the large turbulence levels. The bypass transition mechanism is governed by the entrainment of turbulence into and the subsequent growth of turbulent spots in the laminar boundary layer, and it has been studied in steady and unsteady flow environments both experimentally [**2**] and numerically [**3**, **4**]. In off-design conditions the boundary layer on the suction side of a turbine blade often separates while being still laminar. Laminar separation and transition generally occur where the streamwise pressure gradient changes from favourable or neutral to adverse. This transition mechanism has been modelled successfully by Kwon and Pletcher [**5**] and applied to steady LP turbine flows [**6**]. In the experimental field, Stadtmüller [**7**] measured the off-design flow around a low-speed linear turbine cascade, named T106, with incoming periodic wakes generated by a set of moving bars, in which case the suction-side boundary layer was intermittently separated. The incoming wakes make this test case representative of real operating conditions and challenging for direct numerical simulation (DNS), large eddy simulation (LES) and unsteady Reynolds-averaged Navier–Stokes simulations (URANSs). Two sets of experiments were performed at the University of the Bunderwehr in Munich. In the second set, the wake–blade pitch ratio is a non-integer number, which requires the simulation of more than one vane. Hence, it was decided to simulate one of the experiments from the first set which has a blade–wake pitch ratio, t/t_b, of 2. In such conditions, DNS [**8**], LES [**9**] and URANSs can be performed with reasonable computational effort. The Reynolds number in all the simulations, based on the axial chord length and inlet flow conditions, was set to $Re = 5.18 \times 10^5$.

The MS was received on 31 March 2003 and was accepted after revision for publication on 7 April 2003.

**Corresponding author: Institut für Hydromechanik, Universität Karlsruhe, Kaiserstrasse 12, D-76128 Karlsruhe, Germany.*

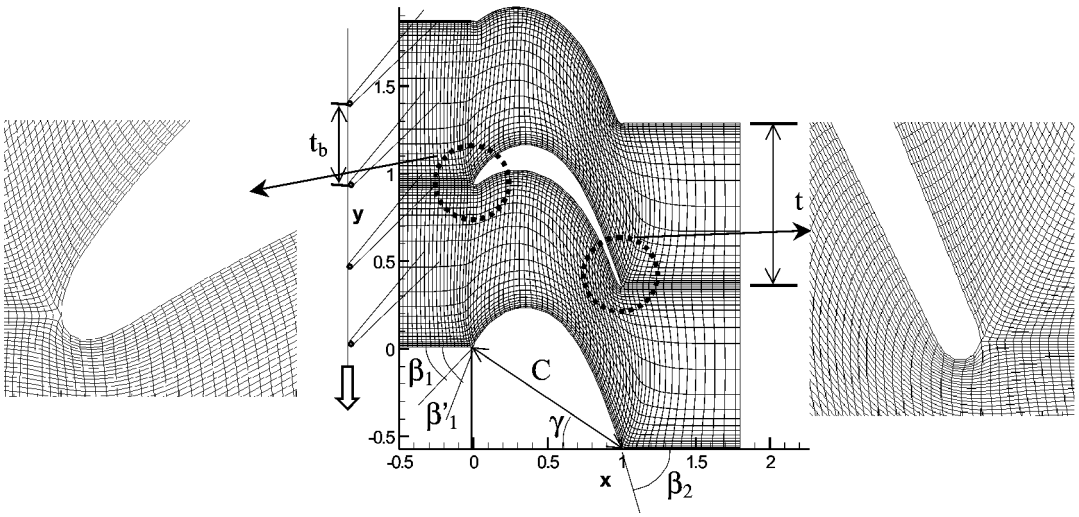

Fig. 1 Grid used for URANSs (every six nodes shown in stream- and pitchwise directions), and zoom of the leading and trailing edge regions (left and right respectively)

2 TEST CASE

The simulations were set up to reproduce the experimental conditions described in reference [**7**]; in the linear test rig the blade aspect ratio, h/C, is 1.76, with $h = 176$ mm, which allows the mid-span section to be considered nearly two-dimensional. The stagger angle, γ, inlet blade angle, β_1, and outlet blade angle, β_2, are 30.72, 37.7 and 63.2° respectively (see Fig. 1), and the inlet and outlet Mach numbers are 0.286 and 0.4. Some difficulties arise in identifying the actual inlet flow angle which is not $\beta_1 = 37.7°$ as designed, but $\beta_1' \cong 45.5°$ as suggested by the RANS simulations performed by Stadtmüller [**7**]. The test rig allows the effect of upstream bladerows to be simulated by a moving bar wake generator, located 70 mm upstream of the leading edge, with a bar diameter–chord ratio of $d_b/C = 0.02$ and a speed of 41.5 m/s. In the numerical simulations, wakes are not generated by bars but by introducing an artificial turbulent wake at the inflow plane. The wake data have been kindly made available by X. Wu and P. Durbin of Stanford University [**3**]. Additionally, the URANSs require the specification of the turbulence length scale, which was set equal to 1 per cent of the blade pitch. The incoming wake mean vorticity is parallel to the blade span, the maximum wake velocity deficit is 25 per cent of the free-stream velocity and the wake half-width is $0.03C$.

3 COMPUTATIONAL METHODS AND SIMULATIONS

Both the DNS and the LES have been performed by using the code LESOCC [**10**]. The code discretizes the incompressible momentum equations using cell-centred finite volumes. To avoid decoupling of the pressure and the velocity fields, the momentum interpolation procedure of Rhie and Chow [**11**] has been applied in the framework of the SIMPLE method to enforce mass conservation. The equations are integrated in time with a three-stage Runge–Kutta algorithm. The subgridscale (SGS) model used in the LES is the dynamic model of Germano *et al.* [**12**].

The URANSs have been carried out by the code XFLOS [**4**], which solves the compressible Navier–Stokes equations by an implicit coupled method that retains second-order accuracy both in space and time. Turbulence is accounted for by the k–ω model [**13**] which allows the equations to be solved down to the solid boundary. To overcome the problem of excessive turbulence production in stagnation regions, the model adopts the 'realizability' constraint in reference [**14**], which reduces the growth of k by clipping the turbulence time scale, $T = k/\varepsilon = 1/\omega$, through the following relation

$$\omega = \frac{1}{T} = \frac{\varepsilon}{k} = \max\left[\omega, \frac{1}{(1/0.09)\sqrt{3/(8|S^2|)}}\right] \tag{1}$$

in which ε is the turbulent dissipation and S is the mean strain.

The measurements, DNS and LES evidenced the presence of a laminar separation bubble on the suction side, which appears in the absence of impinging disturbances and disappears when such disturbances are present. This separation promotes the transition to turbulence of the boundary layer. Therefore, in the URANSs the separated flow transition model described in references [**6**] and [**15**] was implemented. As soon as a separation is detected, transition is switched on when the local momentum thickness Reynolds number, Re_θ, exceeds the critical Reynolds number given by

$$Re_{tr} = \sqrt{\left(1 + \frac{0.05}{\exp(0.365\,Tu)}\right) Re_{\theta,sep}^2 + \frac{17\,000}{\exp(0.509\,Tu)}}$$

Table 1 Overview of the numerical simulations

Simulation	Grid	Turbulence model	Transition model	Realizability	HW	CPU time per processor
DNS [**8**]	1014 × 260 × 64	—	—	—	HSR	64 procs 500 h
LES [**9**]	448 × 144 × 32	Dynamic	—	—	HSR	32 procs 190 h
URANS-01	384 × 144	k–ω	No	Yes	PIII	1 proc. 12 h
URANS-02	384 × 144	k–ω	No	No	PIII	1 proc. 12 h
URANS-03	384 × 144	k–ω	Yes	Yes	PIII	1 proc. 12 h
URANS-04	384 × 144	k–ω	Yes	No	PIII	1 proc. 12 h
URANS-05	384 × 144	k–ω	Yes	Not in separation	PIII	1 proc. 12 h

in which $Re_{\theta,\text{sep}}$ is the momentum thickness Reynolds number at the separation point, and Tu is the turbulence level at the edge of the boundary layer. An intermittency function [**6**, **13**], computed starting from the transition point, multiplies the production rates in both the transport equations for k and ω only inside the boundary layer.

Table 1 summarizes all the reported simulations. Both DNS and LES adopt a three-dimensional grid with 64 and 32 grid nodes over the spanwise extension of 0.2 and $0.15C_{\text{ax}}$ respectively, the suitability of which was carefully checked in references [**8**] and [**9**] by analysing the size of the flow structures revealed by the refined DNS. An essential feature of the grid is the orthogonality close to the walls, which is partly lost close to the leading and trailing edges (see Fig. 1), ensured by an elliptic generation algorithm. The flow is prescribed to be periodic in the spanwise direction. The flow is statistically two-dimensional (the phase-averaged and time averaged span-wise velocity is zero). Hence, the URANSs employ a two-dimensional grid, with the same pitchwise point distribution adopted in LES and with $y^+ < 1.0$–1.9 close to both the blade suction and pressure sides.

In all the simulations the flow is allowed to develop for five periods (one period, T, corresponds to a half-pitch tangential sweep of the wake at the inlet), before a phase-locked averaging procedure is continued for ten extra periods. In the DNS, LES and URANSs, each period is subdivided into 240, 120 and 60 phases, ϕ, respectively.

4 RESULTS

Both DNS and LES have been performed on a Hitachi SR-8000 (HSR) parallel-vector computer, whereas a Pentium III (PIII) was adequate for the URANSs. Table 1 also shows the dramatic differences in the computational effort: the per-processor CPU time ratio between DNS and URANSs can exceed 10^3 when considering processor performance. All the DNS and LES results are reported in two dimensions by a spanwise average of the three-dimensional flowfields.

4.1 Stagnation point anomaly

In the leading edge stagnation region, standard two-equation turbulence models are known to overestimate grossly the turbulent kinetic energy and, consequently, fail to predict the correct boundary layer development downstream. This phenomenon, known as the *stagnation point anomaly*, stems directly from the Boussinesq assumption which, in the presence of strong normal strains, as usually encountered in the deceleration region upstream of the leading edge, predicts too large a production rate of turbulent kinetic energy. To verify how k behaves in the proximity of the stagnation point, it is convenient to plot the time-averaged values of k along the time-averaged stagnation streamline, s (see Fig. 2). The same figure shows how the k profiles predicted by DNS and LES almost coincide. URANS-02 and 04 predict levels of k that are 7 times higher than those

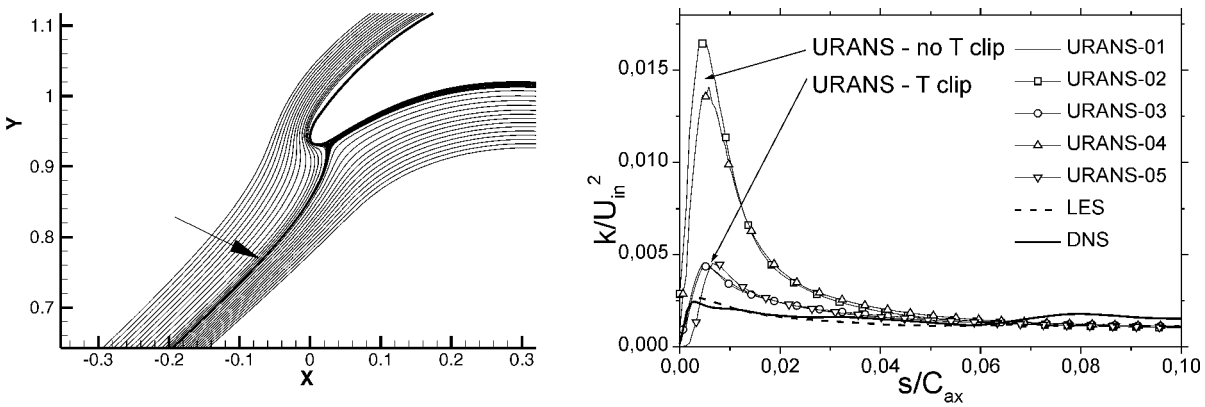

Fig. 2 Left: stagnation streamline (indicated by the black arrow), origin of the streamwise coordinate on blade leading edge. Right: turbulent kinetic energy along the stagnation streamline

given by DNS and LES. When the realizability constraint is enforced (see URANS-01/03/05), the turbulent kinetic energy is reduced, although the peak value is still slightly larger than in the DNS and LES.

4.2 Time and phase averaged flow in the blade vane

Figures 3 and 4 compare the experimental and predicted time-averaged static pressure coefficient, $C_p = 2(p - p_{exit})/U_{in}^2$, and wall shear stress, τ_{wall}. The bars identify the fluctuation ranges obtained in the phase-averaged data. On account of problems in setting the measurement offset [**7**], it is not possible to quantify the magnitude of the wall shear stress and its fluctuation range. Accordingly, the measured values of τ_{wall} have been scaled in magnitude to obtain a sort of *best fit* against the computed values. This allows the comparison of the position of the separation bubble on the suction side and the shape, but not the amplitude, of the wall shear stress fluctuations. The C_p values predicted by DNS and LES are in fairly good agreement with the measurements. On the suction side close to the leading edge, DNS and LES predict lower pressure levels on account of the large incidence angle ($\beta_1' - \beta_1 \cong 7.8°$). This value, suggested by Stadtmüller [**7**] after comparing the experiments with the results of a set of preliminary RANSs, is probably excessive, and in some simulations it is the cause of a small local flow separation for $x/C_{ax} < 0.1$ (see DNS, LES, URANS-03 and 05) which is absent in the measurements. Further downstream, the agreement progressively improves, to be almost perfect for $x/C_{ax} > 0.7$ in the adverse pressure gradient (APG) region. On the pressure side, the flow experiences a strong acceleration which is correctly predicted by all the simulations. Figure 4 shows that URANS-02 and 04 (and URANS-01, not shown here since it is very similar to URANS-02) are in quite good agreement with the measurements. Further URANS calculations at a lower exit Mach number and the same *Re* suggested that the good fit with the measured pressures in the first 50 per cent of the suction side is not to be attributed to compressibility effects, the impact of which is marginal.

The plots also illustrate an interesting feature of the simulations: the C_p and τ_w fluctuation ranges are much larger, and in better agreement with the DNS and experiments, when the realizability constraint is enforced (compare URANS-02/04 with URANS-03/05). When equation (1) is enforced, the predicted C_p slightly deviates from the measurements in the APG region for $x/C_{ax} > 0.6$. URANS-02 predicts no separation on the suction side. A separation appears, although smaller than measured, when switching on the transition model (URANS-04). The best agreement with the experiments is obtained with URANS-03, in which both the realizability and transition models are enforced.

The plots of the time-averaged turbulent kinetic energy of Fig. 5 reveal the absence of any significant turbulent kinetic energy close to the stagnation point for both DNS and LES. This key feature is reproduced by the URANSs that enforce equation (1), while URANS-02 shows how the large values of k close to the stagnation point are convected downstream. Both DNS and LES predict some minor and hardly visible turbulence activity (see the black arrow) in the suction-side boundary layer for $x/C_{ax} < 0.2$–0.3, clearly promoted by

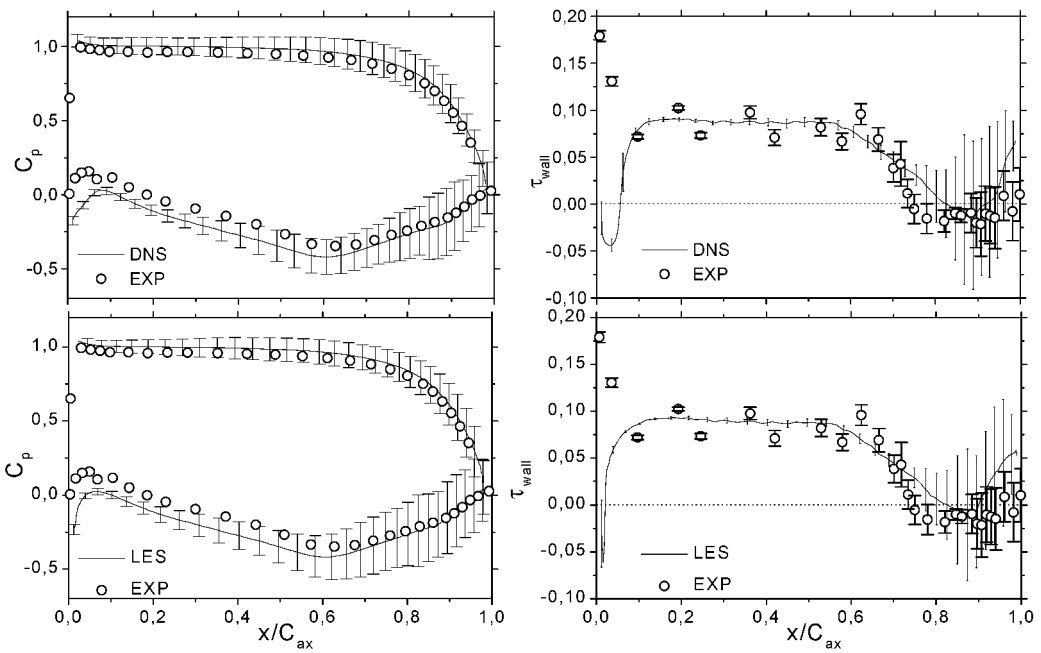

Fig. 3 Static pressure coefficient and suction-side wall shear stress: top DNS, bottom LES

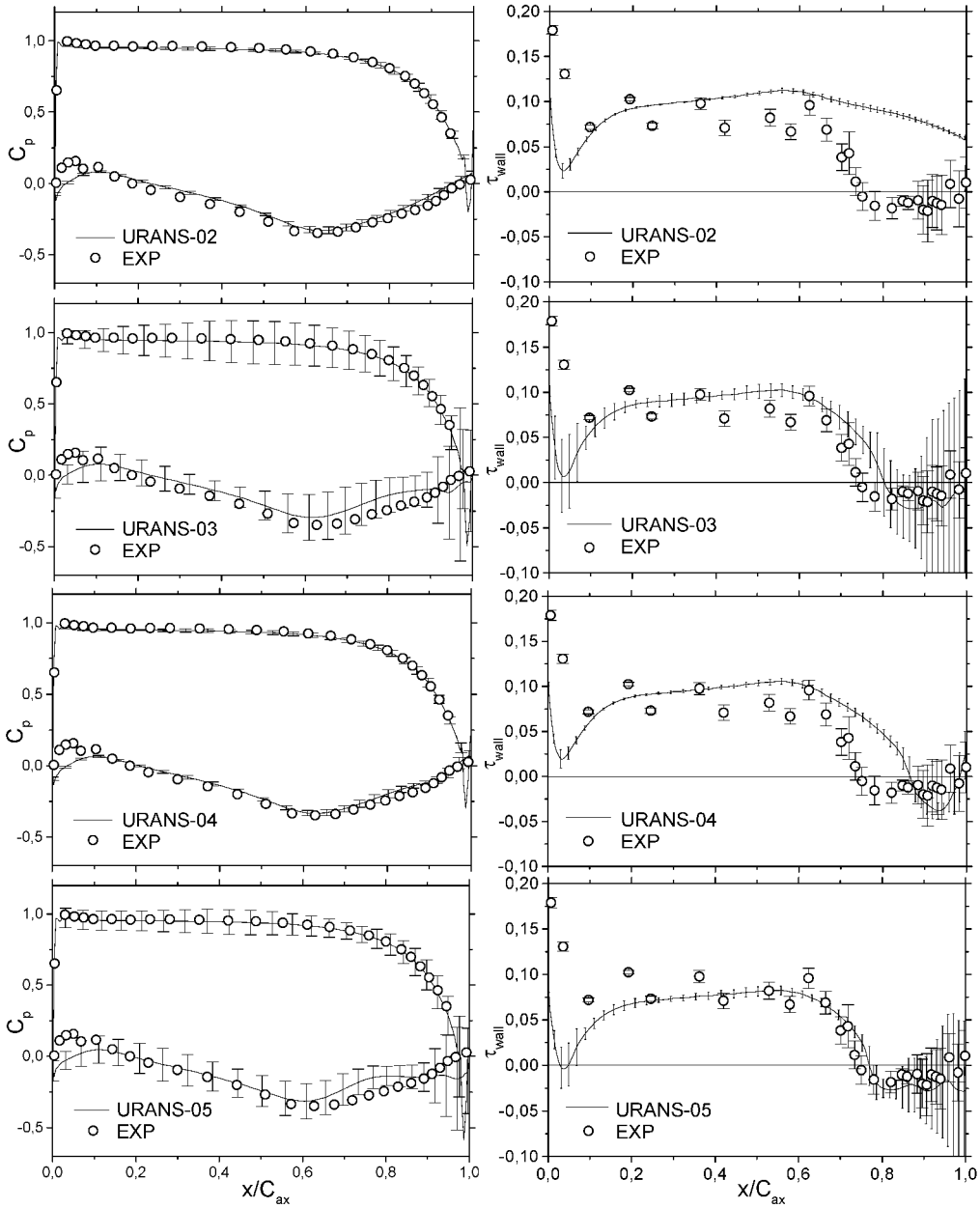

Fig. 4 Static pressure coefficient and suction-side shear stress for various URANSs

the leading edge separation visible in the τ_{wall} plots. For $x/C_{ax} > 0.2$–0.3, k is damped owing to the stretching effect of the strong flow acceleration. The turbulent kinetic energy rises again further downstream, approximately in the separated flow region identified by the wall shear stress plots. The flow picture given by LES is remarkably similar to DNS. Only the concerted action of equation (1) and the transition model allows the URANSs to predict a leading edge separation (see Fig. 4: URANS-03 and 05), which is absent in URANS-02 and 04 (the latter, not shown since it is very similar to URANS-02, enforces the transition model, while the former does not). In general, the URANS do not predict any leading edge transition, i.e. no turbulence production inside the boundary layer upstream of the massive separation in the APG region. URANS-03 reveals the absence of any significant turbulence activity in the stalled region (see Fig. 5), in contrast to both DNS and LES. Apparently, the complex growth and decay of vortices in the stalled region produces flow patterns with large values of mean strain S so that equation (1) predicts exceedingly large values of ω which prevent the growth of k. The obvious cure to this is to switch off equation (1) in the stalled region: the results (see URANS-05) are qualitatively in excellent agreement with DNS and LES, although the extent of the turbulent region in the pitchwise direction is excessive. This improvement in the turbulent kinetic energy pattern is

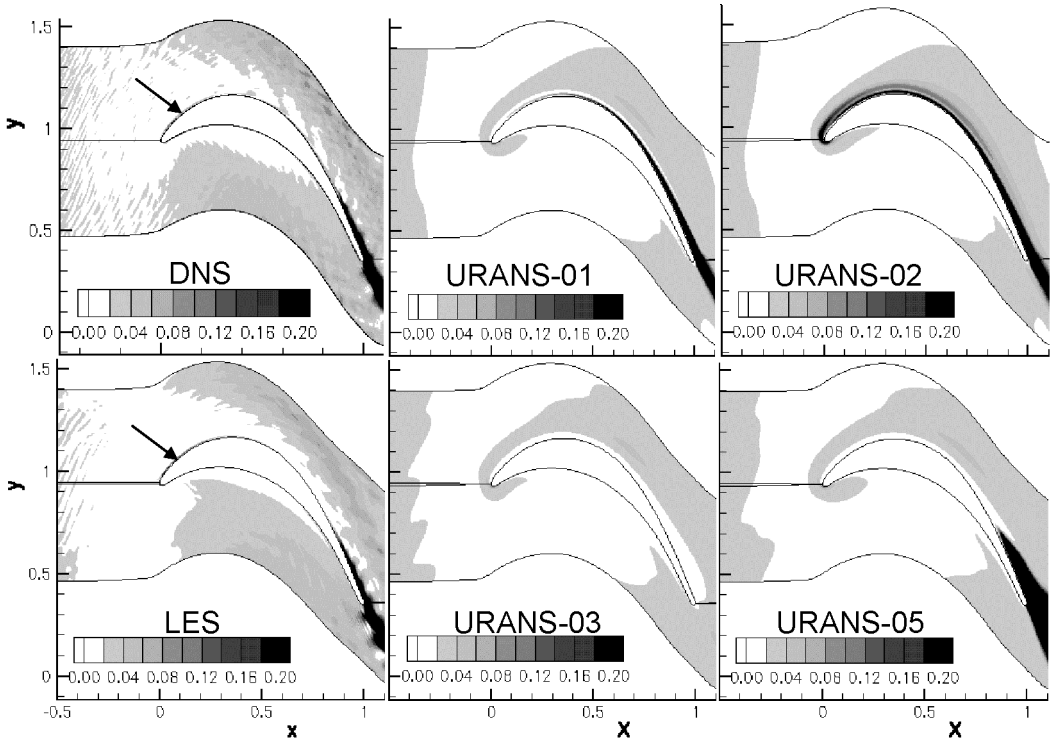

Fig. 5 Time-averaged turbulent kinetic energy, k*10

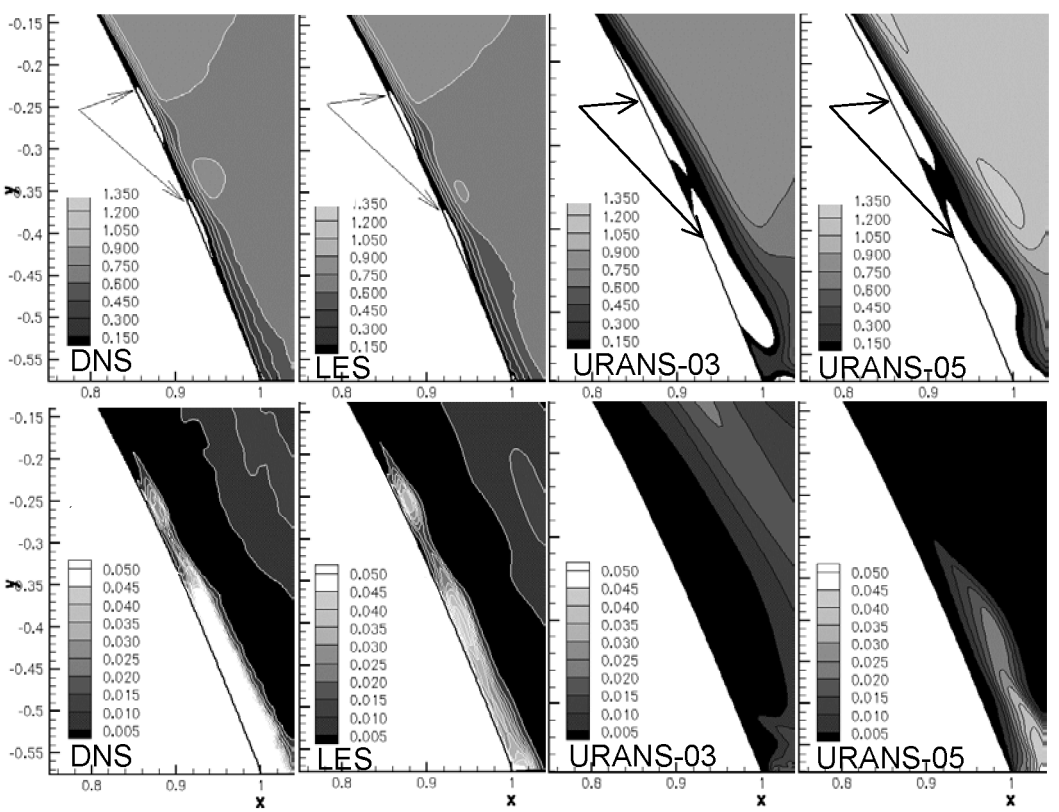

Fig. 6 Phase-averaged axial velocity (top) and turbulent kinetic energy (bottom); white areas indicated by arrows (top) are the reverse flow regions

obtained at the expense of a slightly worse fit of the pressure distribution around the blade, as visible in the C_p plot of URANS-05 in Fig. 4 for $x/C_{ax} > 0.8$–0.85.

4.3 Details of the phase-averaged wake dynamics and boundary layer on the suction side

Both DNS [**8**] and LES [**9**] show the growth of a separation bubble on the suction side. After some time, the shear layer rolls up into two distinct bubbles, as illustrated by the reverse flow areas in Fig. 6, which are conveniently identified by negative axial velocity areas, most likely due to a Kelvin–Helmholtz instability. The turbulent kinetic energy increases downstream of the separation point, thereby showing that the laminar separation triggers transition. In the following phases, not shown here, the two bubbles are convected downstream and dissipate owing to the local increase in k. Of the various URANSs, URANS-03 and 05, which adopt both equation (1) and the transition model, predict a similar pattern. As in the DNS and LES, a laminar separation bubble splits into two bubbles, though with different size and dynamics. The two-dimensional nature of the URANSs yields larger separation bubbles which survive longer owing to the lack of spanwise diffusion. This is a well-known problem of two-dimensional simulations, and the similar results obtained with URANS-03 and 05 indicate the insensitivity of this phenomenon to the realizability constraint. The latter simulation, in which equation (1) is switched off in the separated flow region, shows slightly larger values of turbulent kinetic energy downstream of the second separation bubble. The first bubble does not manage to promote enough entrainment and/or local production.

The dynamics of the wake is illustrated in Fig. 7, which suggests a fair qualitative agreement between the three phase-averaged k isolines predicted by URANS-05 with both the DNS and LES: the plots clearly show how turbulent diffusion increases from DNS to URANSs. Since the LES plots report only the resolved stresses, the peak levels are slightly smaller than in the DNS. For all the simulations, the wake is first slowly bent close to the pressure side ($\phi = 0.0$), where there is a minor increase in k. At $\phi = 0.4$ the wake has already been swallowed into the vane, and some differences arise with the URANSs, which predict a larger diffusion. A slight growth in k close to the pressure side (see the black arrows at $\phi = 0.4$) is predicted by all the simulations. The large levels of k in the bow apex of the wake, observed

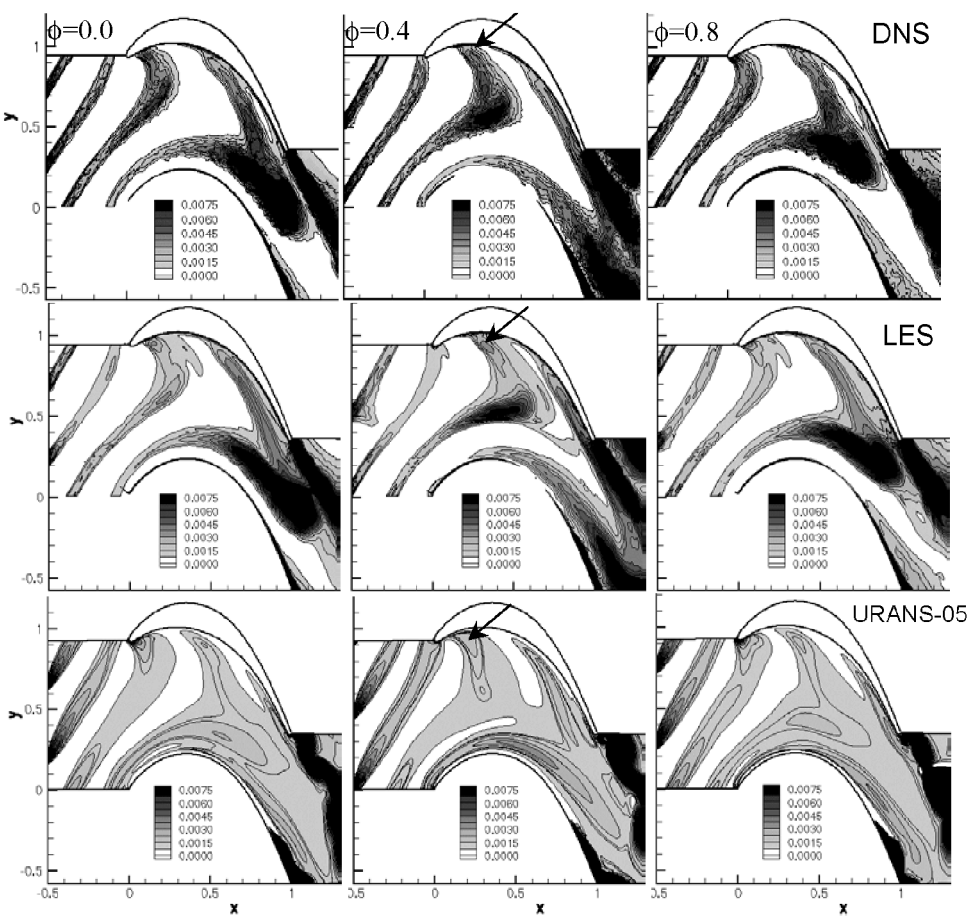

Fig. 7 Turbulent kinetic energy at $\phi = 0.0$, 0.4 and 0.8; top DNS, middle LES, bottom URANS-05

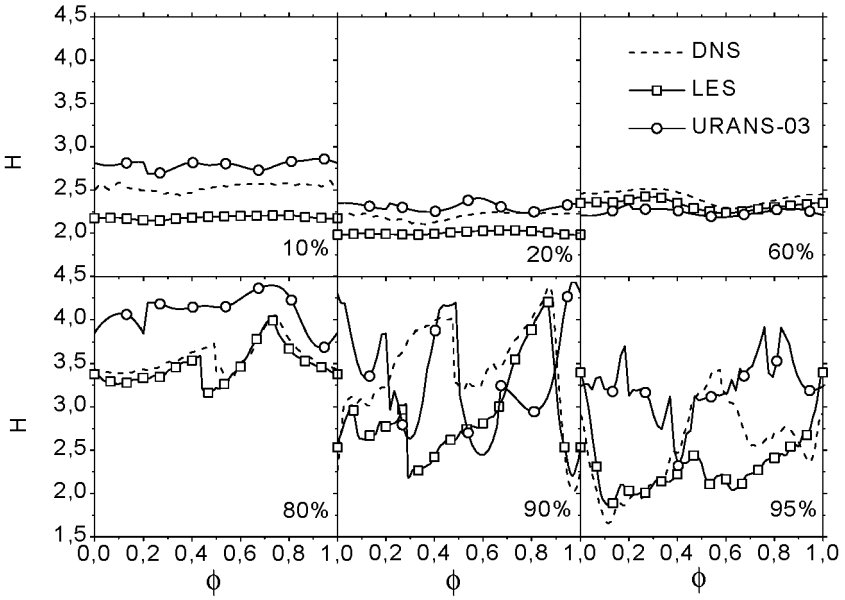

Fig. 8 Phase-averaged shape factor on the suction side at six axial locations

already in the DNS [**8**], are predicted by the LES, and appear clearly in the URANSs only in the subsequent phase ($\phi = 0.8$), although clustered towards the suction side rather than in the blade vane.

Figure 8 shows the phase-averaged shape factor in six axial locations on the suction side (the results of URANS-05 are very similar and are not reported here). The presence of the incoming wake is revealed by the local dips of H at $x/C_{ax} = 0.1$. In the first three sections (10–20–60 per cent) the agreement of the three simulations is satisfactory, again on account of the limited effect of the incoming wakes owing to the strong flow acceleration. In fact, Fig. 7 shows how in the three simulations the large k core, visible in the bow apex of the wake, manages to reach the suction-side boundary layer only for $x/C_{ax} > 0.6$. At $x/C_{ax} = 0.8$, although the overall trend is similar, the shape factor predicted by URANSs is slightly higher because the boundary layer remains laminar for slightly longer (see also Fig. 6). Further downstream ($x/C_{ax} = 0.9$–0.95), turbulence has settled and, although the dynamics of the bubbles predicted by URANSs is different from DNS and LES, the overall agreement is fairly satisfactory.

4.4 Time-averaged total pressure losses

The time-averaged kinetic loss, defined as $\zeta = (P_{0\text{-inlet}} - P_{0\text{-exit}})/(P_{0\text{-inlet}} - P_{\text{inlet}})$, is measured along a cross-section at $0.4C_{ax}$ downstream of the blade trailing edge. This important parameter, which results from the complex blade–wake interaction mechanism, is compared with the experiments in Fig. 9. DNS and LES reproduce the measurements with remarkable accuracy, in spite of the incompressible nature of the simulations. The URANS-02/03/04 are almost

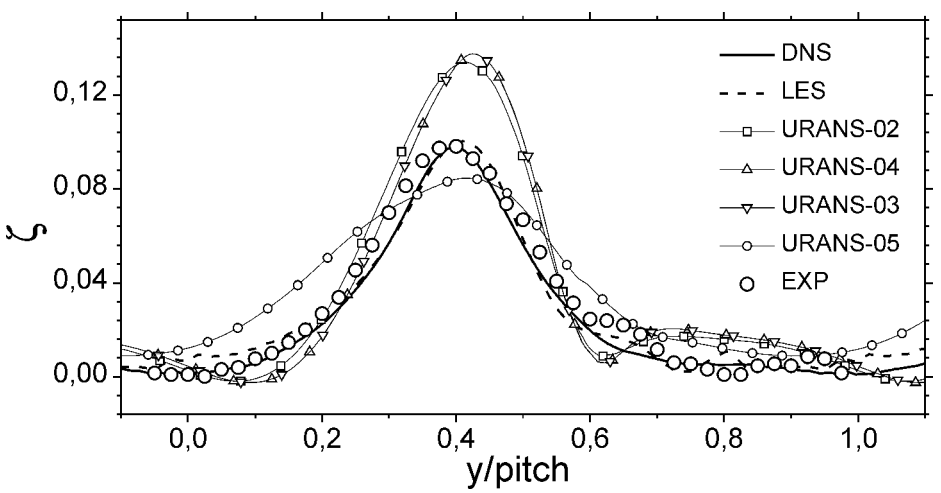

Fig. 9 Kinetic loss coefficient at $0.4C_{ax}$ downstream of the trailing edge

indistinguishable and exhibit a deeper and narrower wake with respect to the experiments. Apparently, the averaged wake is very similar without a transition model (URANS-02, the suction-side boundary layer remains attached) and with a transition model (URANS-03/04, suction-side stall). The situation changes for URANS-05, which includes the transition model and switches off the realizability constraint in the separation bubble, since the wake is smeared out on account of the thicker boundary layer at the trailing edge and the larger production rate of turbulent kinetic energy.

5 CONCLUSIONS

Incoming periodic wakes interact with a laminar separation bubble on the suction side of the blade, making this test case particularly challenging for URANSs. URANSs provide a fair reproduction of the periodic unsteady flow in the LP turbine passage, although the flow pattern details revealed by both DNS and LES are partly lost, especially for the wake dynamics and close to the blade suction side. The stagnation point anomaly in URANSs can be successfully cured by clipping the turbulence time-scale. In spite of the consequent reduction in turbulent kinetic energy, the boundary layer undergoes an early transition to turbulence compared with DNS and LES. Transition can be delayed only by the introduction of a separated-flow transition model. The concerted action of transition and realizability models (the latter switched off in the separated flow region) provides the best accuracy. Both DNS and LES, the details of which are not presented here, evidenced large spanwise flow gradients which promote extra mean strain and production of turbulence resulting in a reduction in the size of the stalled region and earlier reattachment. Since the Reynolds-averaged simulation is intrinsically two-dimensional, URANSs are unable to reproduce the effect of such instantaneous spanwise gradients. Therefore, the exclusion of the realizability constraint in the separated flow region can be seen as a means of promoting production of turbulence in a region where spanwise gradients are lost. It is now possible to conclude that the superior data quality by DNS, which requires no models, can provide vital information for developing and/or tuning existing SGS and RANS models. URANSs need to be used, and improved, on account of the tremendous reduction in computational effort compared with DNS and LES, as summarized in Table 1.

ACKNOWLEDGEMENTS

The authors wish to express their gratitude to the German Research Foundation (DFG) for funding this project, and also to the steering committee of the Super Computing facilities in Bavaria (HLRB) for granting computing time on the Hitachi SR8000-F1 in Munich to perform DNS calculations and to the steering committee of the Computer Centre of the University of Stuttgart for providing computing time on the Hitachi SR8000-F1 in Stuttgart to perform the LES calculation.

REFERENCES

1 **Mayle, R. E.** The role of laminar-turbulent transition in gas turbine engines. *Trans. ASME, J. Turbomach.*, 1991, **113**, 509–537.
2 **Liu, X.** and **Rodi, W.** Experiments on transitional boundary layers with wake-induced unsteadiness. *J. Fluid Mechanics*, 1991, **231**, 229–256.
3 **Wu, X., Jacobs, R. G., Hunt, J. R. C.** and **Durbin, P. A.** Simulation of boundary layer transition induced by periodically passing wakes. *J. Fluid Mechanics*, 1999, **398**, 109–153.
4 **Michelassi, V., Martelli, F., Dénos, T., Arts, T.** and **Sieverding, C. H.** Unsteady heat transfer in stator–rotor interaction by two equation turbulence model. *Trans. ASME, J. Turbomach.*, 1999, **121**, 436–447.
5 **Kwon, O. K.** and **Pletcher, R. H.** Prediction of incompressible separated boundary layers including viscous–inviscid interaction. *Trans ASME, J. Fluids Engng*, 1979, **101**, 466–472.
6 **Rodi, W.** and **Schönung, B.** Interaktives-Inverses Grenzschichtverfahren zur Berechnung von lokalen Ablöseblasen an Turbinenschaufeln. *Z. Flugwiss. Weltraumforsch.*, 1987, **11**, 271–280.
7 **Stadtmüller, P.** Investigation of wake-induced transition on the LP turbine cascade T106A-EIZ. DFG-Verbundproject Fo 136/11, Version 1.0, 2001.
8 **Wissink, J. G.** DNS of a separating low Reynolds number flow in a turbine cascade with incoming wakes. 5th International Symposium on *Engineering Turbulence Modelling and Measurements*, Mallorca, Spain, September 2002, 16–18.
9 **Michelassi, V., Wissink, J. G.** and **Rodi, W.** Analysis of DNS and LES of a low-pressure turbine blade with incoming wakes and comparison with experiments. Report 789, Institute for Hydromechanics, University of Karlsruhe, Germany, 2002.
10 **Breuer, M.** and **Rodi, W.** Large eddy simulation for complex turbulent flows of practical interest. *Flow Simulation with High Performance Computers II, Notes on Numerical Fluid Mechanics*, 1996 (Wieweg-Verlag, Braunschweig).
11 **Rhie, C. M.** and **Chow, W. L.** Numerical study of the turbulent flow past an airfoil with trailing edge separation. *Am. Inst. Aeronaut. Astronaut. J.*, 1983, **21**, 1525–1532.
12 **Germano, M., Piomelli, U., Moin, P.** and **Cabot, W. H.** A dynamic subgrid-scale eddy viscosity model. *Phys. Fluids A* 1991, **3**(7), 1760–1765.
13 **Wilcox, D. C.** Reassessment of the scale-determining equation for advanced turbulence models. *Am. Inst. Aeronaut. Astronaut. J.*, 1988, **26**, 1299–1310.
14 **Durbin, P. A.** On the k–ε stagnation point anomaly. *Int. J. Heat and Fluid Flow*, 1996, **17**, 89–90.
15 **Michelassi, V.** Shock-boundary layer interaction and transition modelling in turbomachinery flows. *Proc. Instn Mech. Engrs, Part A: Power and Energy*, **211**, 1997.